INTERNATIONAL JOURNAL OF INTEGRATED ENGINEERING
ISSN: 2229-838X e-ISSN: 2600-7916

IJIE

Vol. 17 No. 6 (2025) 224-234
https://publisher.uthm.edu.my/ojs/index.php/ijie

Design and Fabricate of 3D Printed X-Band Sample Size Based Polyethylene Terephthalate Glycol (PETG) Rectangular Waveguide

Muhammad Zulfauzan Fahmi Che Alias[1], Herdawatie Abdul Kadir[1,2]*, Fahmiruddin Esa[3], Huda A. Majid[4], Nur Nazifa Mod Arsad[1], Iffan Darwis Mohd Ibrahim[1], Babul Salam Ksm Kader Ibrahim[5]

[1] *Faculty of Electrical and Electronics Engineering, Universiti Tun Hussein Onn Malaysia (UTHM), Parit Raja, Batu Pahat, Johor, 86400, MALAYSIA*
[2] *Research Centre for Applied Electromagnetic, Institute of Integrated Engineering (I2E), Universiti Tun Hussein Onn Malaysia (UTHM), Parit Raja, Batu Pahat, Johor, 86400, MALAYSIA*
[3] *Department of Physics and Chemistry, Faculty of Applied Sciences and Technology, Universiti Tun Hussein Onn Malaysia (UTHM), Parit Raja, Batu Pahat, Johor, 86400, MALAYSIA*
[4] *Advanced Telecommunication Research Center (ATRC), Universiti Tun Hussein Onn Malaysia (UTHM), Parit Raja, Batu Pahat, Johor, 86400, MALAYSIA*
[5] *Department of Electrical and Computer Engineering, College of Engineering and Architecture, Gulf University for Science & Technology, Masjid Al Aqsa Street, Mubarak Al-Abdullah P.O.Box 7207, Hawally, KUWAIT*

*Corresponding Author: watie@uthm.edu.my
DOI: https://doi.org/10.30880/ijie.2025.17.06.018

Article Info

Received: 30 May 2025
Accepted: 16 September 2025
Available online: 30 December 2025

Keywords

Waveguide' 3D printing, infill density, infill pattern, PETG

Abstract

This work discusses the design and fabrication of 3D-printed dielectric materials for rectangular waveguides, with specific attention given to the effects of infill density and pattern changes on dielectric attributes. Microwave CST Studio is used to design the waveguide structures, which were produced through additive manufacturing and later tested with a two-port rectangular waveguide measurement system. The S-parameters were measured using a Keysight PNA-L Network Analyzer N5234B, whereby the reflection coefficient (S11) and the transmission coefficient (S21) were measured to determine how the material interacts with electromagnetic waves. It was found that greater infill densities correlated with increased values of real permittivity, whereas infill patterns have an essential influence on the material's dielectric behavior. Several patterns were tested: concentric, cross, cubic, and zigzag; the zigzag pattern gave the best results concerning the effective permittivity, while the concentric pattern presented the least because of the greater air gaps. The strong dependence of permittivity on infill density was observed across 9-12Hz with average R^2 values of 0.96, confirming the possibility of controlling dielectric properties through additive manufacturing using PETG material. It has been demonstrated that 3D printing methods can fabricate waveguides and RF circuits that enable control over dielectric properties.

1. Introduction

Waveguides are a fundamental part of microwave systems, transmitting electromagnetic waves with minimal losses. Traditional manufacturing processes often constrain the complexity of waveguide designs. The conventional method for characterizing the s-parameter/permittivity of composite material in microwave application measurement is using a two-port waveguide [1].

Generally, the sample under test is prepared via casting and compacted powder in a waveguide [2-3]. There are some drawbacks, especially in the processes that must be done before transmission line measurement. For instance, in casting technique, the prepared sample needs to go through surface treatment, ensuring that the surface is flat enough so that it is perpendicular to the wave propagation, which takes a lot of time [4]. At the same time, the compacted powder method tends to fail due to the air gap occurring between the particles, which makes it fragile, resulting in inaccurate data. Hardened samples could be improved by heat treatment at high temperatures; however, this process will cause a change in overall dimensions due to the shrinkage effect of an enhanced grain boundary [5-7]. Therefore, it will create an airgap between the waveguide wall and the sample, which can also contribute to inaccurate data.

On the other hand, 3D printing can realize complex geometrical shapes that improve waveguide performance by optimizing other parameters such as radiation patterns and impedance matching [8]. Currently, the adoption of 3D printing for the fabrication of waveguides has gained more interest due to its capability to adopt complex geometries and rapid prototyping [9-10]. However, by using the 3-D printing method, some parameters need to be investigated, such as infill density, infill pattern, material/filament used, printing resolution, etc.

Thus, this work will investigate infill density and pattern, which could possibly affect the waveguide's permittivity properties [11-15]. Polyethylene terephthalate glycol (PETG) will be used in the Microwave CST Studio for simulation and 3D printing for fabrication. The effect of different infill densities and patterns on waveguide performance is also studied.

2. Design And Fabrication

In this work, a 3-D rectangular object was created based on X-band waveguide dimensions: height 10.16 mm, width 22.86 mm, and thickness 5 mm, which is less than a quarter wavelength at 10 GHz. Figure 1 shows the X-band waveguide sample size using CST Microwave Studio. The 3-D file will be exported in.stl for further processing.

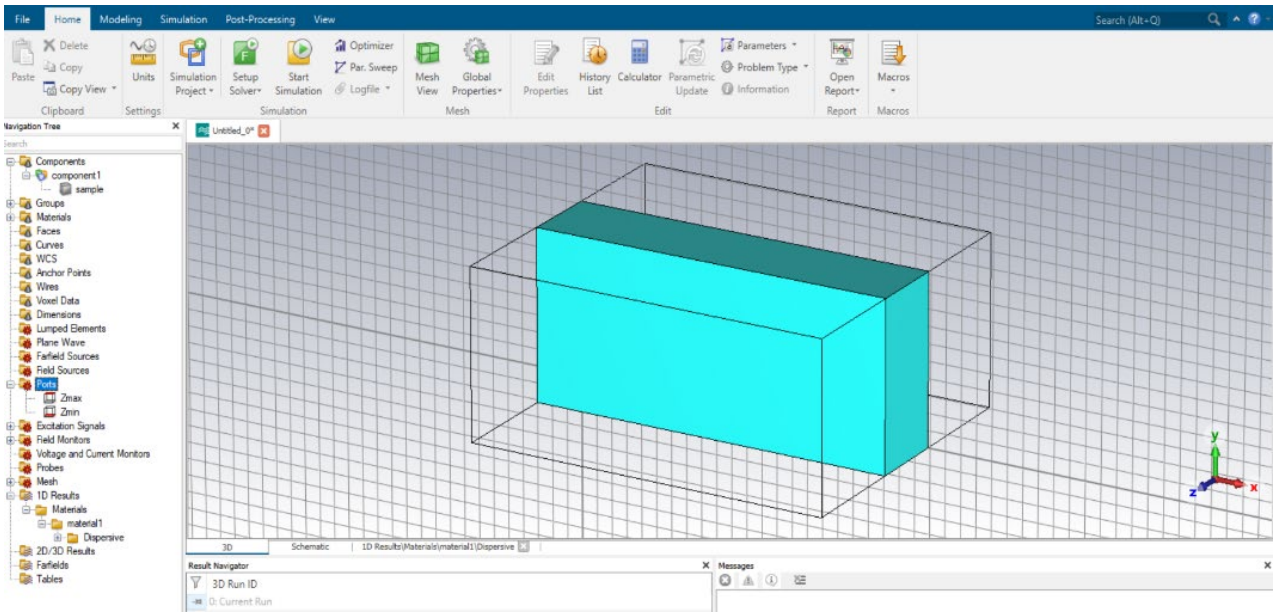

Fig. 1 *Designation of X-band waveguide sample size*

Exported 3-D file in .stl was later opened via Ultimaker Cura 5.8 software for slicing as shown in Figure 2. Various infill densities (in %) and patterns were made in this process. Different infill patterns will distribute forces affecting waveguide performance via strength and flexibility [16-19].

Int. Journal of Integrated Engineering Vol. 17 No. 6 (2025) p. 224-234

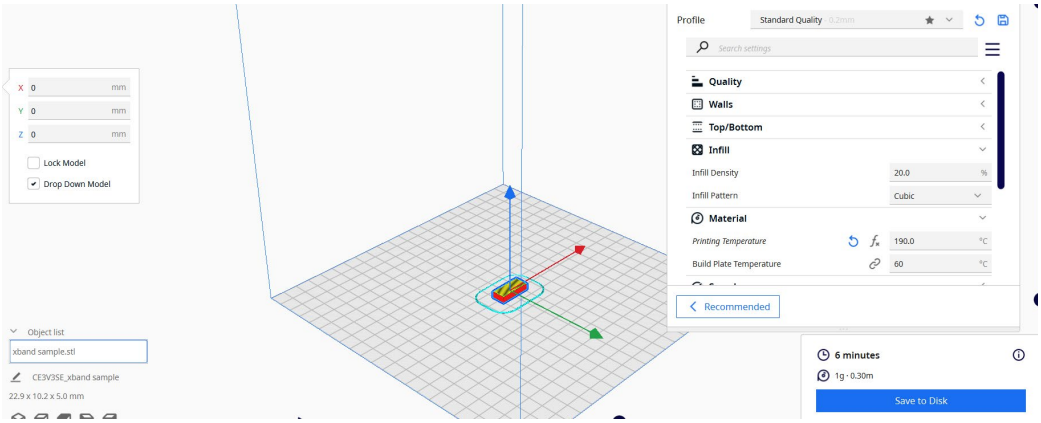

Fig. 2 *Printing setup for slicing and G-code conversion using the Ultimaker Cura software before 3-D printing*

Figure 3 shows the chosen fill densities of 20%, 40%, 60%, and 80% for the rectangular waveguide that was designed using computer software. The selected fill densities correspond to various volumetric material distributions in the 3D-printed PETG structure, which affect its dielectric properties and electromagnetic performance. Lower fill volumes (20% and 40%) generate bigger voids in the structure, which may lower the effective permittivity of the structure and increase transmission losses due to high impedance mismatch.

On the other hand, higher fill volumes (60% and 80%) permit better continuous material distribution, resulting in better wave propagation and impedance matching. Determining the relationship between fill percentage and S-parameter response can be used with simulation and fabrication to enhance material properties for microwave devices. Software-designed waveguide models offer control over fill patterns and densities, which provides consistent results between differing material configurations.

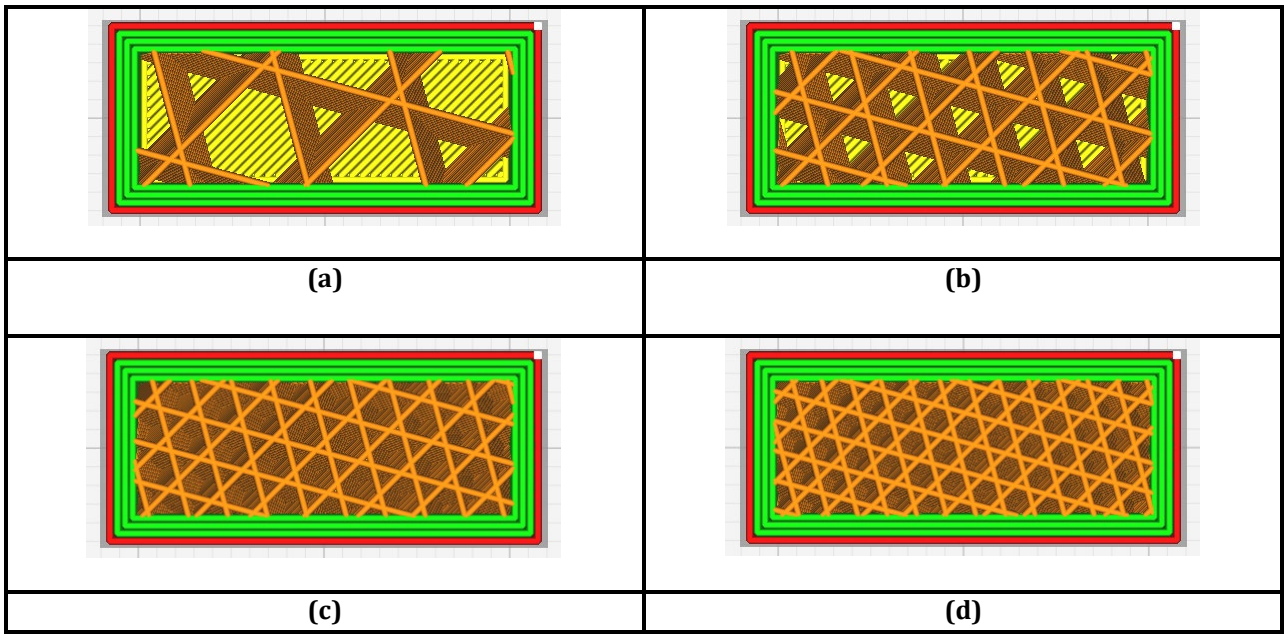

Fig. 3 *Infill density (%) taken after 21 slices: (a) 20 %; (b) 40 %; (c) 60 %; and (d) 80 %*

The infill patterns in this study were concentric, cross, cubic, and zigzag. These patterns were chosen for the analysis due to the X-band design, which provides uniform strength in all directions. Maintaining structural integrity and ensuring consistent electromagnetic performance across different environmental conditions is crucial. Figure 4 represents a sample of the visual representation of the pattern for the design of a rectangular waveguide for an infill pattern at 60% density. The slices were made after 21 layers of cuts to achieve cross-sectional representation of the internal structure. These patterns were selected due to their geometrical characteristics, which have a direct impact on material distribution, interlayer adhesion, and overall density

uniformity. By visualising the patterns throughout this intermediate slicing stage, the morphology impact of every infill pattern can be better understood and equated to the electrical and mechanical performance.

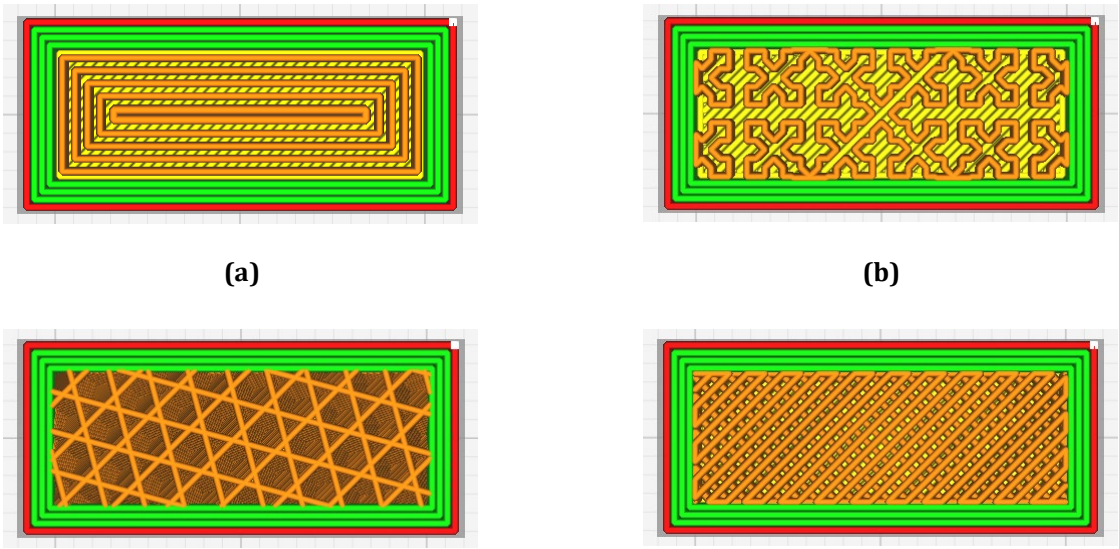

(a) **(b)**

(c) **(d)**

Fig. 4 *Various infill (60%) patterns taken after 21 slices: (a) concentric; (b) cross; (c) cubic; and (d) zigzag*

As shown in Figure 5, the X-band size 3-D printed sample was fabricated with a two-port adapter setup for testing purposes. S-parameter measurements were performed to accurately define the X-band frequency range response of the 3D printed PETG samples with the PNA-L Network Analyzer N5234 B. S-parameter analysis will reveal vital information regarding the electromagnetic characteristics of 3D printed PETG substrates, confirming the dielectric properties that are amenable to modification through controlled changes in infill density.

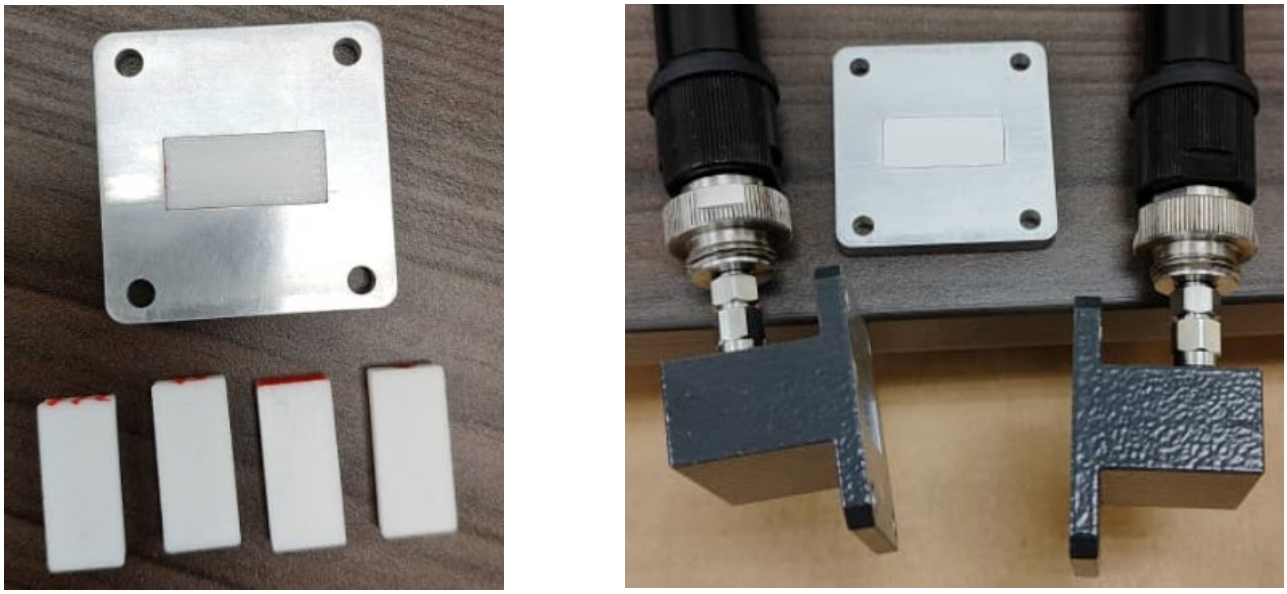

(a) **(b)**

Int. Journal of Integrated Engineering Vol. 17 No. 6 (2025) p. 224-234

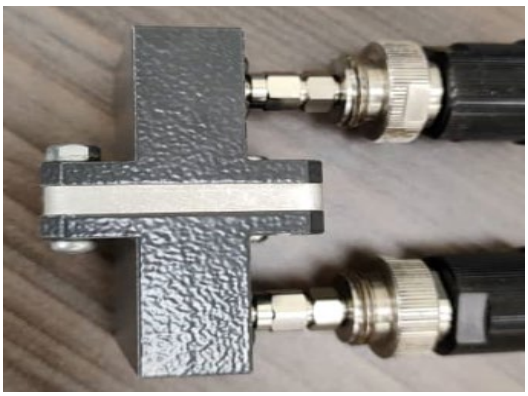

(c)

Fig. 5 *(a) X-band size 3-D printed sample; (b) 3-D printed sample inside the X-band waveguide with two-port adapters; (c) two-port waveguide configuration*

3. Results

Figure 6 demonstrates the influence of infill density on the microwave characteristics of 3D-printed Polyethylene Terephthalate Glycol (PETG) samples within the X-band frequency range (8.5 GHz to 12 GHz). The primary parameters examined are the S11 (reflection coefficient) and S21 (transmission coefficient, which elucidate the reflection and transmission properties of the samples at different infill densities.

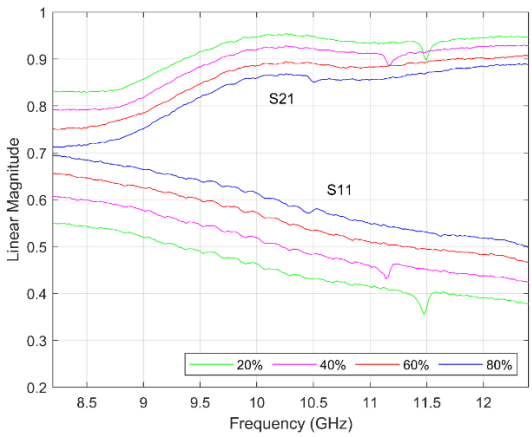

(a)

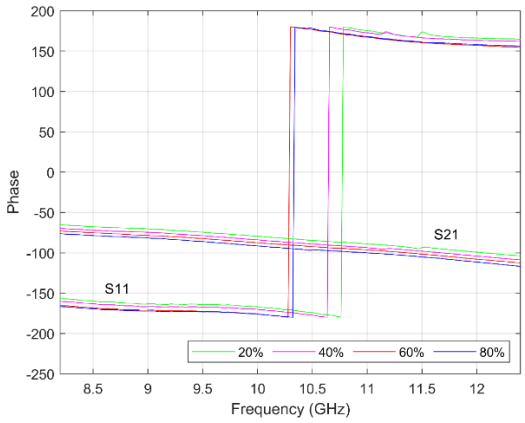

(b)

Fig. 6 *S-parameters (a) Linear magnitude; and (b) phase of various infill densities*

The reflection coefficient (S11) represents the ratio of incident electromagnetic (EM) energy that is reflected due to impedance mismatch. Elevated infill densities (80%) demonstrate increased S11 values, signifying that more energy is reflected instead of being absorbed or transmitted through the material. This is due to the elevated material density, which leads to enhanced effective permittivity and diminished impedance matching with open space [8] . Reduced infill densities (20%) exhibit diminished S11 values, indicating improved impedance matching and superior absorption properties. The reduced density facilitates increased wave penetration and scattering within the material, decreasing overall reflection. A significant decline in S11 is detected at approximately 11.5 GHz, signifying a resonance phenomenon where energy absorption reaches its peak. It may result from constructive and destructive interferences within the material's microstructure, affecting the infill density. The findings indicate that low-infill structures (20%-40%) are preferable for microwave absorber applications, where reflection minimization is essential. In contrast, higher infill densities (60%-80%) are more appropriate for applications necessitating increased reflectivity, such as electromagnetic shielding or wave-guiding structures.

The transmission coefficient (S21) indicates the extent of power transmission through the material. As infill density escalates, S21 diminishes, suggesting that samples with greater density attenuate the transmitted signal more efficiently. This results from heightened dielectric losses and absorption linked to denser material structures. The highest S21 values are recorded at 20% infill density, signifying that a substantial fraction of the electromagnetic wave is passed through the structure without attenuation. The 80% infill sample demonstrates the lowest S21 values, indicating that a minimal portion of the wave is transmitted due to heightened material density and associated dielectric loss. A broad upward trend in S21 is detected across the frequency range, with deviations near 11.5 GHz, corresponding to the resonant behavior noted in S11. From an application standpoint, low-density infill structures (20%-40%) are beneficial in situations necessitating wave transparency, such as radomes and dielectric substrates for antenna applications. In contrast, elevated infill densities (60%-80%) are advantageous for shielding applications, where the reduction of signal penetration is essential.

Elevated infill densities exhibit marginally more pronounced phase changes, attributable to enhanced dielectric loading and impedance mismatch effects. S21 (Transmission Phase Shift): A notable phase shift (~180 degrees) is detected between 10.5 and 11 GHz, indicating a resonance state. This shows a significant material interaction at this frequency, potentially resulting from wave interference phenomena within the infill structure. The change in phase response over diverse infill densities indicates that altering density can effectively tune electromagnetic phase properties, which is advantageous for applications including phase shifters, impedance-matching structures, and frequency-selective surfaces (FSS). The fluctuations in S11 and S21 throughout the frequency spectrum demonstrate that material response is frequency-dependent [12]. It underscores the necessity of customizing infill parameters according to the operational frequency of the proposed microwave applications.

Figure 7 displays the complicated permittivity characteristics of Polyethylene Terephthalate Glycol (PETG) samples within the X-band frequency range (8.5 GHz to 12 GHz), accounting for various infill densities (20%, 40%, 60%, and 80%). On the other hand, Table 1 shows the relationship between permittivity and infill density.

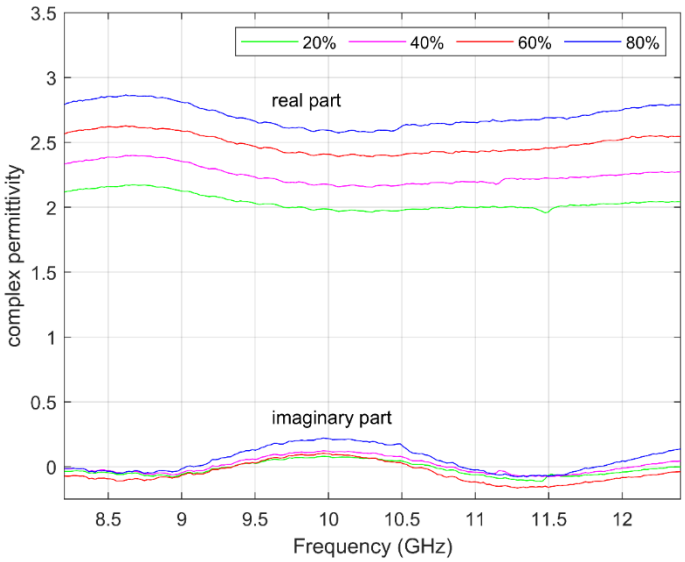

Fig. 7 *Complex permittivity against frequency for various infill densities*

The infill densities of 80% demonstrate the highest values; this trend is anticipated, as augmenting the infill density incorporates additional dielectric material, resulting in an elevated total permittivity. All samples exhibit

Int. Journal of Integrated Engineering Vol. 17 No. 6 (2025) p. 224-234

a peak between 10 and 11 GHz, signifying a frequency-dependent loss mechanism. It may result from relaxation processes or resonance within the polymeric structure. Notwithstanding this peak, the overall dielectric loss remains negligible, indicating that PETG is a comparatively low-loss material, appropriate for microwave applications where little energy dissipation is required. For applications necessitating elevated permittivity (e.g., antennas, microwave lenses, and high-dielectric substrates), an infill density of 80% is advised.

Table 1 *Relationship between permittivity and infill density*

Frequency (GHz)	Permittivity of various infill densities			
	20%	40%	60%	80%
9	2.124	2.354	2.587	2.810
10	1.984	2.175	2.408	2.592
11	1.998	2.196	2.426	2.654
12	2.029	2.250	2.522	2.750

Figure 8 presents the linear relationship between permittivity and infill density, showing a clear trend where permittivity increases with higher infill density. The results indicate a highly linear correlation between permittivity and infill density, represented by a correlation coefficient near (R^2 = 0.99) for all frequencies tested. This implies that permittivity predictably increases with higher infill density due to the increased volume fraction of dielectric material, which is consistent with the dielectric mixture. It provides a straightforward method for adjusting electromagnetic properties, where precise control of permittivity is crucial for optimizing performance.

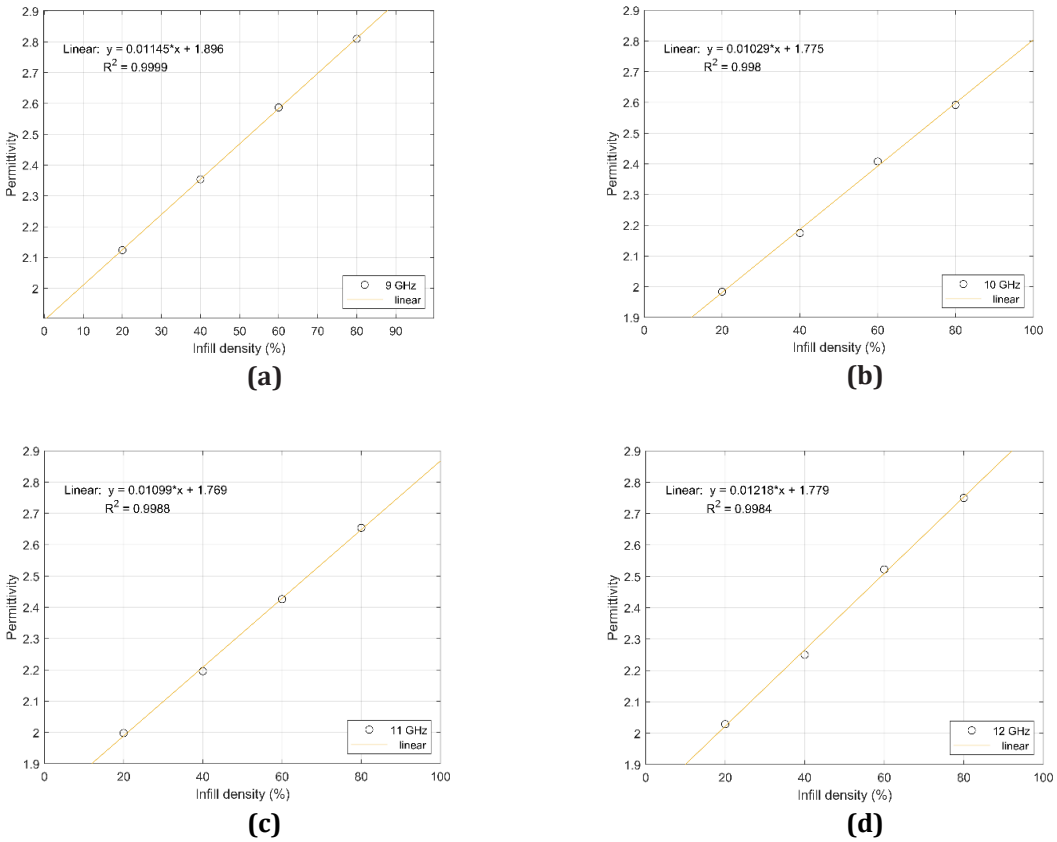

Fig. 8 *Linear relationship between permittivity and infill density: (a) 9GHz; (b) 10 GHz; (c) 11 GHz; (d) 12 GHz*

The S-parameters (S11 and S21) for the concentric, cross, cubic, and zigzag infill patterns reveal how the inner structural composition modifies the microwave response of the 3D-printed rectangular waveguide, as shown in Figure 9. The results show the difference in reflection (S11) and transmission (S21) coefficients at the range of 8.5 GHz to 12 GHz, which considers the interaction of the electromagnetic waves with the structure, which is strongly dependent on the geometry of the infill. The results from the analysis show that the choice of infill pattern directly impacts the dielectric and microwave transmission properties of the 3D printed waveguide structures. Of all the

configurations tested, the cubic and cross infill patterns are the best candidates for applications where low reflection and high transmission properties are desirable, as they performed the best in both S_{11} and S_{21}.

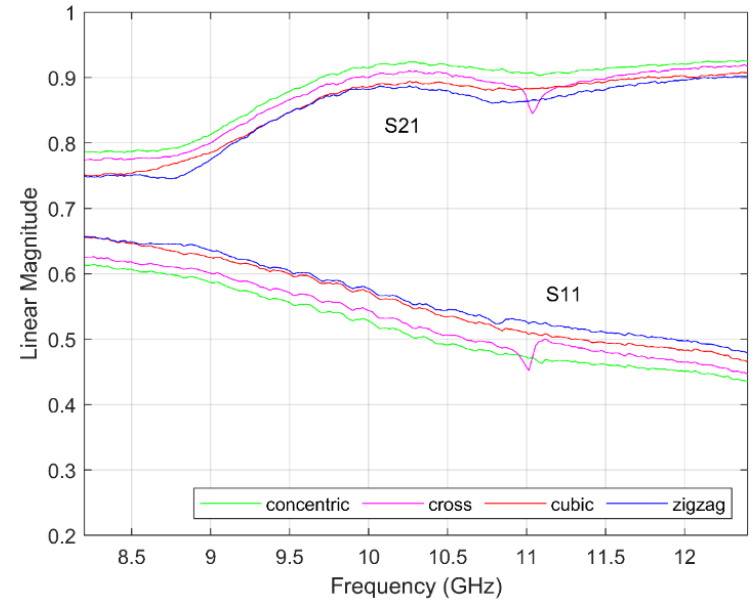

(a)

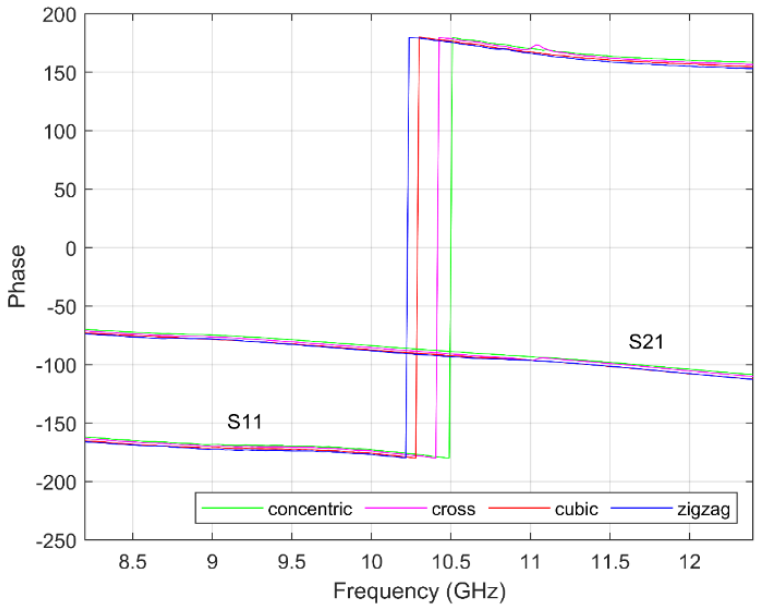

(b)

Fig. 9 *S-parameters (a) Linear magnitude; and (b) phase of various infill patterns*

Figure 10 shows the complex permittivity values captured for the concentric, cross, cubic, and zigzag infill patterns. The results show the real part ranging from 2.0 to 2.8, with the cubic and cross patterns having more pronounced values while imaginary counterparts being relatively low throughout the frequency spectrum, showing little dielectric losses. The differences suggest the internal structural geometry affects the effective permittivity; wherein more uniform and denser infill designs are achieved, increased dielectric constants are obtained because lower quantities of air voids and higher degrees of material homogeneity are present. Table 1 shows the relationship between permittivity and infill density.

Int. Journal of Integrated Engineering Vol. 17 No. 6 (2025) p. 224-234

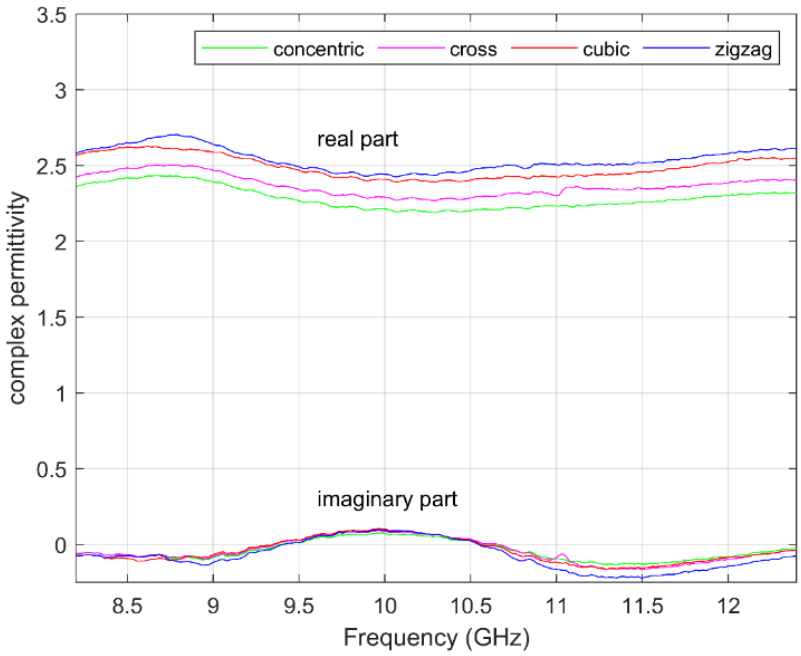

Fig. 10 *Complex permittivity against frequency for various infill patterns*

The relations between infill patterns and corresponding permittivity are shown in Figure 11 with a high R^2 value, which means there is a strong predictability of the permittivity changes with different infill structures [17, 20]. The shape of a zigzag has the maximum permittivity due to increased material and low air volume fraction. These findings enhance the understanding of the effects of infill geometry on 3D-printed dielectric materials and the performance of devices composed of these functional electromagnetic devices.

Table 2 *Relationship between permittivity and infill pattern*

Frequency (GHz)	Permittivity of various infill patterns			
	concentric	cross	cubic	zigzag
9	2.392	2.469	2.587	2.640
10	2.212	2.291	2.408	2.442
11	2.233	2.302	2.426	2.507
12	2.301	2.385	2.522	2.578

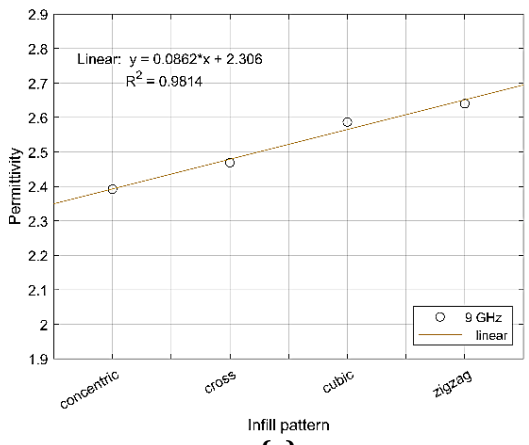

(a)

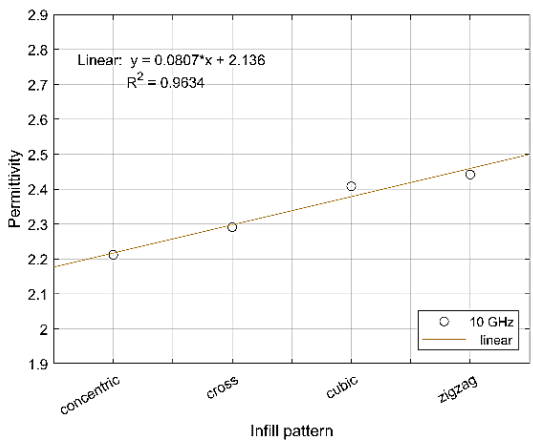

(b)

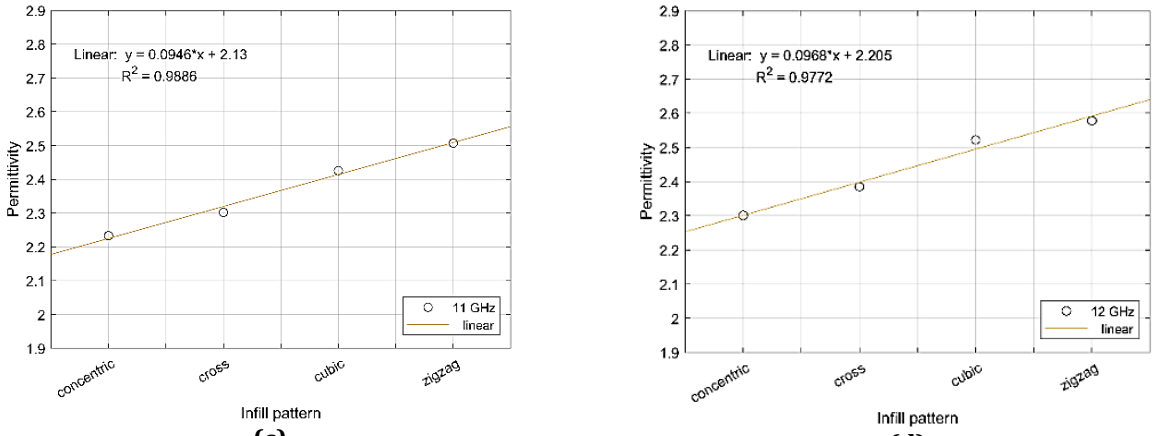

Fig. 11 *Linear relationship between permittivity and infill pattern: (a) 9GHz; (b) 10 GHz; (c) 11 GHz; (d) 12 GHz*

4. Conclusion

This research successfully designed, fabricated, and tested a 3D-printed rectangular waveguide structure to determine the effects of infill density and patterns on dielectric properties. Experimental outcomes validate that higher infill densities correspond to greater real permittivity, while the infill pattern significantly changes the material's dielectric response. Of all inverted patterns tested, the zigzag structure had the highest effective permittivity, while the concentric pattern had the lowest due to possessing a greater amount of air. The strong correlation further validates the dependence of permittivity on infill density, confirming that additive manufacturing provides unprecedented control over dielectric properties and is thus applicable for customizable electromagnetic uses.

The S-parameters from the fabricated two-port rectangular waveguide structures were measured, and the results from the S11 and S21 responses for the different infill configurations show some differentiation. The differences in reflection and transmission coefficients prove that 3D-printed waveguide materials can be designed to have controlled electromagnetic characteristics, which indicates that they can be used for RF, microwave, and communication systems. This research also emphasizes the possibility of additive manufacturing as a fast-prototyping technique for creating functional dielectric materials with designed parameters.

Acknowledgement

This research was supported by Universiti Tun Hussein Onn Malaysia (UTHM) through Multidisciplinary Research Grant (MDR) (vot Q693) and Postgraduate Research Grant (vot J042).

Conflict of Interest

Authors declare that there is no conflict of interests regarding the publication of the paper.

Author Contribution

The authors confirm contribution to the paper as follows: ***Original Draft Preparation and Writing:*** *Muhammad Zulfauzan Fahmi bin Che Alias,* ***Conceptualization:*** *Nur Nazifa Mod Arsad;* ***Methodology:*** *Nur Nazifa Mod Arsad, Fahmiruddin Bin Esa;* ***Software:*** *Nur Nazifa Mod Arsad;* ***Supervision:*** *Herdawatie Abdul Kadir, Huda A. Majid;* ***Validation:*** *Herdawatie Abdul Kadir, Huda A. Majid;* ***Writing-Reviewing and Editing:*** *Herdawatie Abdul Kadir;* ***Writing-Reviewing:*** *Fahmiruddin Bin Esa, Iffan Darwis Mohd Ibrahim;* ***Testing:*** *Fahmiruddin Bin Esa. All authors reviewed the results and approved the final version of the manuscript.*

References

[1] Orend, K. & Musch, T. (2024) S-Parameter Characterization Based on Dielectric Waveguides in D-Band, *2024 15th German Microwave Conference (GeMiC),* 167-170. IEEE.

[2] Bunea, A.C., Neculoiu, D. & Dinescu, M.A. (2022) Characterization of 3-port SAW diplexers using 2-port VNA measurements, *2022 International Semiconductor Conference (CAS),* 81-84. IEEE.

[3] Plüss, T., Zimmer, F., Hehn, T. & Murk, A. (2022) Characterisation and comparison of material parameters of 3D-printable absorbing materials, *Materials,* 15(4), 1503.

[4] Moghaddam, M.K., Khosrownejad, M. & Fleury, R. (2022) Ultra-Compact Ka-band Metamaterial Waveguide Filters, Fabricated by Lost-Wax Casting, *2021 51st European Microwave Conference (EuMC),* 269-272. IEEE.

[5] Sanchez-Olivares, P., Ferreras, M., Garcia-Marin, E., Polo-López, L., Tamayo-Domínguez, A., Córcoles, J., Fernández-González, J.M., Masa-Campos, J.L., Montejo-Garai, J.R., Rebollar-Machain, J.M. & Ruiz-Cruz, J.A. (2022) Manufacturing guidelines for W-band full-metal waveguide devices: Selecting the most appropriate technology, *IEEE Antennas and Propagation Magazine,* 65(2), 48-62.

[6] Nawrot, W., Bartsch, H., Szostak, K., Słobodzian, P., Müller, J. & Malecha, K. (2022) Ceramic Additive Manufacturing for High-Performance Microwave Circuits, *2022 24th International Microwave and Radar Conference (MIKON),* 1-4. IEEE.

[7] Ja'afar, P. N., Idrus, S. M., Ambran, S., Yusri, N. A., Mohamed, N., Hamzah, A., .& Hayashi, T. (2023). Metallic Cylinder Reflected Power Measurement for 93.1 GHz Frequency Modulated Continuous Wave Radar Calibration. International Journal of Integrated Engineering, 15(3), 187-192.

[8] Zou, J., Müller, S., Lücken, V. & Diewald, A.R. (2024) Methods of Measuring Permittivity and Permeability of 3D-Printed Samples in a Rectangular Waveguide, *2024 25th International Microwave and Radar Conference (MIKON),* 249-253. IEEE.

[9] Pons-Abenza, A., Arregui, I., Laso, M.A., Lopetegi, T. & Martin-Iglesias, P. (2024) Design of an Additively-Manufactured Self-Supported All-Metal Coaxial-Line X-band Bandpass Filter, *IEEE Access*.

[10] Goode, I. & Saavedra, C.E. (2022) 3D printed linearly polarized X-band conical horn antenna and lens, *IEEE Open Journal of Antennas and Propagation*, 3, 549-556.

[11] Maidin, S., Ting, K. H., & Sim, Y. Y. (2022). Investigation of mechanical properties of recycled ABS printed with open source FDM printer integrated with ultrasound vibration. International Journal of Integrated Engineering, 14(4), 57-63.

[12] Kattel, B., Hutchcraft, W.E. & Gordon, R.K. (2023) Exploring infill patterns on varying infill densities on dielectric properties of 3D printed slabs, *2023 Antenna Measurement Techniques Association Symposium (AMTA),* 1-5. IEEE.

[13] Kattel, B., Ayan, U., Mohoppu, M., Villacorta, B. & Hutchcraft, W.E. (2024) Enhancing permittivity of 3D printing filaments via nanocompounding for electromagnetic applications*, SoutheastCon 2024*, 1016-1021. IEEE.

[14] Kattel, B., Hutchcraft, W.E. & Gordon, R.K. (2025) Evaluating the Relationship between Relative Permittivity and Infill Density in 3D Printed Dielectric Slabs, *IEEE Access*.

[15] Shaik, K. Z. (2022). CPW-fed microstrip patch antenna for millimeter wave applications. International Journal of Integrated Engineering, 14(7), 69-83.

[16] Carvalho, S. S., Reis, J. R., Mateus, A., & Caldeirinha, R. F. (2024). Exploring design approaches for 3D printed antennas. IEEE access, 12, 10718-10735.

[17] Tayeb, G., Burokur, S. N., Yahiaoui, R., & Wu, B. (2021). 3D-printed antennas: A review of technologies, techniques, and applications. Additive Manufacturing, 46, 102154.

[18] Wirth, S. G., Morrow, I. L., & Horsfall, I. (2019). Fabrication procedure and performance of 3D printed X-band horn antenna. In Loughborough Antennas & Propagation Conference (LAPC 2018) (pp. 1–5). IEEE.

[19] Karakoç, M. C., & Şahin, A. B. (2020). Development of 15-dB Gain Conical Horn Antenna Using 3D Printing Technology. Electrica, 20(2), 177–181.

[20] Ma, Z., Feng, L., Zhou, H., Hu, W., & Zhang, Y. (2023). Fabrication of the Designed Horn Antenna Using 3D Printing Technology. In 2023 International Conference on Microwave and Millimeter Wave Technology (ICMMT) (pp. 1-3). IEEE.